Fermi level tuning using the Hf-Ni alloy system as a gate electrode in metal-oxide-semiconductor devices

Jonathan Avner Rothschild,[a] Aya Cohen, Anna Brusilovsky, Lior Kornblum, Yaron Kauffmann, Yaron Amouyal, and Moshe Eizenberg
Department of Materials Engineering, Technion – Israel Institute of Technology, Haifa 32000, Israel

(Received 28 February 2012; accepted 22 May 2012; published online 13 July 2012)

Hf-Ni alloys are studied as a gate electrode for metal-oxide-semiconductor devices. The Hf-Ni solid-state amorphization couple encompasses several metallurgical phenomena which are investigated at the nanoscale and are correlated with the macroscopic electrical properties of devices. The dependence of the Fermi level position on the alloy composition is studied both on SiO_2 and on HfO_2. In order to isolate the effects of interfacial and dielectric charges and dipoles, the dependence of the vacuum work-function values on the composition is also studied. The Fermi level positions of the alloys do not depend linearly on the average composition of the alloys and are strongly affected by Hf enrichment at the $HfNi_x$/dielectric interface and the $HfNi_x$ surface. We note a constant shift of 0.4 eV in the Fermi level position on HfO_2 compared to SiO_2. In addition, characterization of the composition, structure, and morphology reveals Kirkendall voids formation when the bottom layer consists of Ni, and an oxygen-scavenging effect when the bottom layer is Hf. © *2012 American Institute of Physics*. [http://dx.doi.org/10.1063/1.4730618]

I. INTRODUCTION

In the recent few years, the building block of modern microprocessors—the metal oxide semiconductor field effect transistor (MOSFET)—is undergoing significant changes in the microelectronics industry. Unacceptably high leakage currents, caused by the constant scaling of dimensions, have necessitated the replacement of the traditional polycrystalline-Si/SiO_2 gate stack with metal/high permittivity material (high-K dielectric) stacks.[1,2] Among the most challenging aspects of this replacement is the control of the Fermi level position at the metal electrode/dielectric interface,[3] which in turn controls critical performance parameters of the device, such as the threshold voltage.

For complementary MOS technology in order to enable good performance, the Fermi level position should be parallel to the Si conduction band (~4 eV) for nMOSFET and parallel to the Si valence band (~5.1 eV) for pMOSFET.[1] The dual metal approach using a low work-function metal for nMOSFET and a high work-function metal for pMOSFET is problematic due to materials' problems.[3] The low work-function metals are highly reactive with oxides, and high work-function metals have poor adherence to the oxides. By alloying two or more metals these opposite attributes can be balanced.

Alloying metals with different vacuum work-functions (Φ_M^{Vac}) values have been investigated for Fermi level position control purposes,[4–15] and some alloy systems have demonstrated a wide range of effective work function (Φ_M^{Eff}) values as a function of composition. However, few of these works have investigated the physical aspects of the metal electrode.

An alternative to metal alloys is using a single midgap metal such as TiN or TaN combined with ultrathin (~1 nm) dielectric layers that shift the Φ_M^{Eff} to the necessary ranges. Typically, La oxide is used for nMOSFET and Al oxide for pMOSFET.[16–20] This route has emerged as a better alternative for the current high-k dielectric stack technology. However, future MOSFET technologies might not fit well with this solution.

In this work, we study the Hf-Ni alloy system, where a low work-function metal ($\Phi_{Hf}^{Vac} = 3.9$ eV) is mixed with a high work-function metal ($\Phi_{Ni}^{Vac} = 5.15$ eV).[21] This system has already been studied for its solid state amorphization reaction, which is caused by the difference in mobility between Hf and Ni atoms, the large negative heat of mixing and the difference in atomic volume.[22] An amorphous gate metal is advantageous since the problem that stems from the dependence of work-function on crystallographic orientation, that exists in poly-crystalline metals, is prevented.[23,24] Moreover, in practical devices the grain size may be considerably larger than the actual gate.

Lee *et al.* studied the HfNi/HfO_2 system as a candidate gate stack in MOS devices.[14] Their promising results showed that there is a ~1 eV shift in the flatband voltage between the pure Ni electrode and electrodes where a Hf layer was beneath the Ni layer. However, they could not measure the Φ_M^{Eff} values of the electrode since they could not isolate the effects of oxide charges and dipoles.

In this work, the beveled oxide method is used for the extraction of Φ_M^{Eff} of HfNi alloys both on HfO_2 and SiO_2 dielectrics.[25] Furthermore, charges and dipoles at the high-K/metal interface and inside the high-K stack are known to have an effect on the Φ_M^{Eff} value.[26–29] In order to isolate the contribution of the metal from these effects, the Φ_M^{Vac} values are measured separately from the Φ_M^{Eff} values. A first-principle calculation of the Hf_2Ni intermetallic phase Φ_M^{Vac} is performed in order to explain some of the results. From the

[a]jehonathan@gmail.com.

understanding of the physical-material phenomena, the ability to control the electrical properties of Hf-Ni alloys is obtained over a wide range of Φ_M^{Eff} values.

In addition, we correlate the macroscopic electrical properties of devices using Hf-Ni alloys as a gate electrode with effects of nanoscale metallurgical phenomena, using state of the art analytical techniques such as high resolution transmission electron microscopy (HRTEM) and time of flight secondary ion mass spectrometry (ToF-SIMS).

II. EXPERIMENTAL

A. Materials characterization

The samples for material characterization were prepared on Si (001) wafers with a thick (120 nm) thermally grown layer of SiO_2. The sequential deposition of Hf and Ni was done by e-gun evaporation of pure Hf and Ni targets. In one set of samples, Hf was deposited first and Ni was deposited next to form a Ni/Hf stack on top of SiO_2. Different thickness ratios of this set were deposited. These thickness ratios were calculated to achieve certain compositions according to the atomic density ratio between Hf and Ni, which is 0.49. Another set of samples consisted of three layers—Ni/Hf/Ni. All the samples underwent heat treatments in high vacuum ($<10^{-7}$ Torr) at 300 °C to 700 °C for durations of 30 to 90 min. The samples were characterized by ToF-SIMS for a composition profile using a ION-TOF GmbH TOF.SIMS 5 system. X-ray diffraction (XRD) for structure determination was done using a Philips PW 3710 x-ray Diffractometer system.

Cross-sectional TEM samples from an as-deposited (AD) Ni(91 nm)/Hf(28 nm)/SiO_2 stack were prepared using a dual-beam focused ion beam system (FIB, FEI Strata 400 s). The samples were then attached to a Ti grid in the FIB. Two *in situ* heating experiments were done using a 652 double tilt heating holder (Gatan, Pleasanton, CA, USA) on a FEI Titan 80–300 S/TEM (FEI, Eindhoven, The Netherlands) operated at 300 KeV and equipped with both an image Cs corrector, and a post-column energy filter (Tridiem 866 ERS, Gatan). One experiment was done in a standard Cs-corrected TEM imaging mode and the other one in an energy filtered TEM mode (EFTEM) while elemental mapping the Ni $L_{2,3}$-edge.

B. Work-function measurements

MOS capacitors were fabricated in order to perform capacitance-voltage (C-V) measurements. First, 50 nm of SiO_2 were thermally grown on p-type Si (001) wafers. Afterwards, the SiO_2 was etched using dilute hydrofluoric acid (HF) with a gradient of etching time over the wafer, resulting in a beveled oxide. A thin 4 nm layer of HfO_2 was deposited on some of the wafers by the atomic layer deposition (ALD) method using a Tetrakis(dimethylamino) Hafnium and H_2O precursors in a Cambridge NanoTech "Savannah-200" system. Both "Hf-under" and "Ni-under" (Hf or Ni is the first layer deposited, correspondingly) were deposited through shadow masks using e-gun evaporation. Al was then deposited on the back side of the wafers for electrical back contact. For elemental Ni work-function measurements, pure Ni electrodes were deposited. Since Hf and Hf-Ni alloys oxidize and have poor electrical contacts with the probes, Ni was used as a capping layer in order to improve the electrical contact. Therefore, for elemental Hf work-function measurements a Ni(10 nm)/Hf(90 nm) stack was annealed at 300 °C for 30 min in vacuum strictly for back contact formation and radiation damage healing. We verified that at this temperature no Ni-Hf interdiffusion took place. The rest of the "Hf-under" samples was annealed at 500 °C in order to allow the Ni to diffuse into the Hf layer. The "Ni-under" samples were annealed at 300 °C, at which only the two inner layers intermix and the top layer remains pure Ni. These conditions for the thermal treatment were chosen based on the results of the initial materials characterization of the Hf/Ni system, which are elaborated in the Sec. III.

Capacitance-voltage (C-V) measurements were performed using a probe station sealed from light using an HP 4284 A LCR meter. The ac voltage applied was 25 mV at a frequency of 100 kHz. The areas of the capacitors were measured using a light microscope.

The samples for the complementary Φ_M^{Vac} measurements consisted of six alternating layers—Hf/Ni/Hf/Ni/Hf/Ni deposited on Si (001) wafers with a thick (120 nm) thermally grown layer of SiO_2. All the layers of a specific element had the same thickness while different thickness ratios between the Ni layers and the Hf layers were deposited. The Ni/Hf thickness ratios were 0.12 (20 at. % Ni), 0.26 (35 at. % Ni), 0.49 (50 at. % Ni), 0.91 (65 at. % Ni), and 1.96 (80 at. % Ni). The samples underwent thermal treatment at 500 °C for 1 h in high vacuum ($<10^{-6}$ Torr). The Φ_M^{Vac} measurements were done using a Besocke Kelvin Probe (KP) S system with a Kelvin control 07, which was constructed in a vacuum chamber connected to a sputtering system. Since the Hf-Ni alloys oxidize at the surface, the samples were briefly sputtered with Ar^+ prior to the measurement. In addition, a built-in oven was used in order to bake the samples immediately after sputtering at 300 °C for 5 min in order to bring the surface to a steady-state. The KP measurements were taken before and after the heating and showed no substantial difference within the experimental error.

Selected samples were further characterized by TEM imaging and high-angle annular dark field scanning transmission electron microscopy (HAADF-STEM) imaging with energy dispersive spectroscopy (EDS) line scans for a composition profile.

III. RESULTS AND DISCUSSION

A. Basic metallurgical results

Figure 1 shows the ToF-SIMS profiles of a Ni(45 nm)/Hf(55 nm)/SiO_2 sample after heat treatments at various temperatures, showing no observable intermixing between Hf and Ni at 300 °C. A peak related to oxygen (Cs_2O^+) is observed exactly at the Ni/Hf interface both in the as-deposited sample and in the sample after the 300 °C anneal. There is also some O in the bulk of the Hf layer, with an estimated concentration of 5–10 at. % O. The existence of this O peak can explain the lack of inter-diffusion at this temperature. The two layers fully intermix and the O peak disappears after the 500 °C anneal. In addition, in this

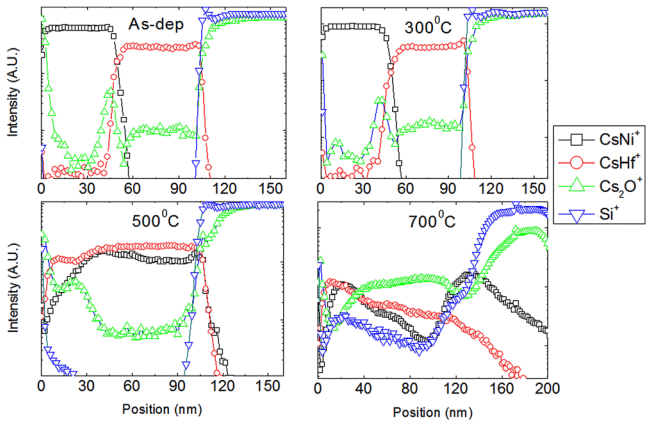

FIG. 1. ToF-SIMS profiles of a Ni(45 nm)/Hf(55 nm)/SiO_2 sample as deposited and after 1 h of anneal in vacuum at 300 °C, 500 °C, and 700 °C.

temperature O is apparent in the surface layer up to a depth of 30 nm, where there is some excess Hf. This is attributed to the formation of HfO_2 in this region and is supported by XRD peaks related to HfO_2. At 700 °C, there is a strong reaction between Hf and SiO_2 which results in the formation of monoclinic HfO_2 and reduced Si which forms with Ni the silicide Ni_2Si.

Figure 2 illustrates another type of interface between the Ni and Hf layers, where the Hf is evaporated on top of the Ni layer. This is a Ni(60 nm)/Hf(40 nm)/Ni(10 nm)/SiO_2 sample which exhibits an O peak at the Ni/Hf interface but not at the inner Hf/Ni interface. Now we observe that the intermixing through the Hf/Ni interface begins at a temperature as low as 300 °C, while no such intermixing occurs in the upper Ni/Hf interface up to 450 °C. In other samples without an Hf/Ni interface, the lowest temperatures in which intermixing is observed is also at 450 °C. This indicates a correlation between intermixing and the O peak, which can be explained by the evaporation process. In the Ni/Hf interface, the time that it takes for the Hf target to cool down and for the Ni target to heat up for evaporation is long enough for an ultrathin layer of native oxide to form on the surface of the Hf layer even in the high vacuum conditions ($\sim 10^{-7}$ Torr) at the evaporation chamber. This native oxide inhibits the

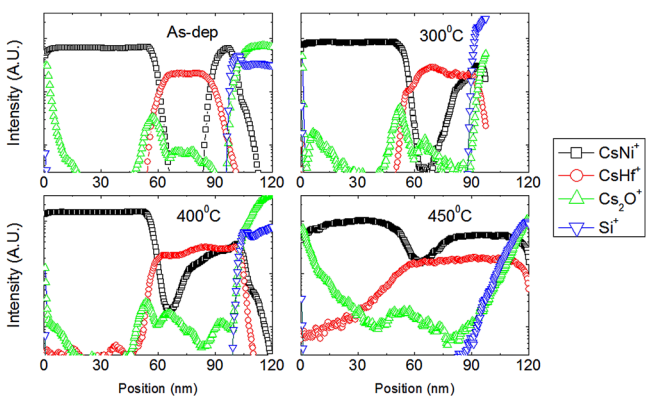

FIG. 2. ToF-SIMS profiles of a Ni(60 nm)/Hf (40 nm)/Ni(10 nm)/SiO_2 sample as deposited and after 1 h of anneal in vacuum at 300 °C, 400 °C, and 450 °C.

diffusion at temperatures lower than 450 °C. This O peak is not formed at the Hf/Ni interface since now Ni is deposited first and then Hf is deposited, and on Ni a native oxide is not formed so easily.

In order to obtain a quantitative analysis of the Ni concentration, the samples for Φ_M^{Vac} measurements were used as calibration to the EDS. The cross-section TEM micrographs of samples after thermal treatment are presented in Fig. 3 showing that for lower Ni concentrations there is a complete mixture, but for the sample which contains a nominal concentration of 80 at. % Ni (Fig. 3(c)), there are thin layers which do not mix. These layers consist of pure Ni as shown in the line profile of integrated EDS signal of Ni taken across the sample, see Fig. 4(a). Figure 4(b) shows the calibration between the average EDS integrated intensity of Ni and the actual Ni average concentration determined by the layers thicknesses and atomic densities. The average EDS intensity for the nominal 80 at. % Ni sample was taken excluding the pure Ni layers. The reason that some of the Ni remains unmixed is that Ni is the dominant diffusing species.[30,31] The maximal amount of Ni that can penetrate the $HfNi_x$ solid solution is determined by the composition in which the amorphous solid solution, which is in equilibrium with pure Ni, is not stable according to the free energy diagram of Ref 17. This corresponds to a composition of approximately 78 at. % Ni, confirming our EDS findings. Heat treatment experiments done on the Ni(91 nm)/Hf(28 nm) sample at 500 °C for 30, 60, and 90 min show that the mixing and the residual Ni layer thickness are almost invariant to the time of heat treatment and the Ni/HfNi stack remains stable, further supporting this argument.

XRD peaks associated with the Hf_2Ni phase are clearly observed in the Ni(30 nm)/Hf(70 nm)/SiO_2 sample after the 500 °C thermal treatment, while for higher concentrations of Ni, no significant peaks of any $HfNi_x$ intermetallic phases are observed. In addition, a microstructure of uniform distribution of fine grains is observed in the lower Ni concentration TEM samples, as seen in Fig. 4(a). The formation of Hf_2Ni in $HfNi_x$ alloys with compositions from 0 to 40 at. % Ni can be explained by the free energy diagram in Ref. 16, since the amorphous phase is not stable at these compositions. The semi-stability of the amorphous phase in $HfNi_x$ alloys with compositions between 40 and 78 at. % Ni is in agreement with re-crystallization experiments done on bulk amorphous $HfNi_x$ samples with various compositions, which showed that the re-crystallization temperatures are expected to be above 500 °C.[32]

B. Capacitance decrease in "Ni-under" samples

A substantial decrease in the accumulation capacitance (C_{Acc}) is observed in Ni/Hf(20 nm)/Ni(50 nm) and Ni/Hf(35 nm)/ Ni(35 nm) stacks deposited both on SiO_2 and on HfO_2, as shown in Fig. 5. C_{Acc} is assumed to be equal to the oxide capacitance which is according to a parallel plate capacitor approximation

$$C_{Acc} = \frac{K_{SiO_2}\varepsilon_0 A}{EOT}, \quad (1)$$

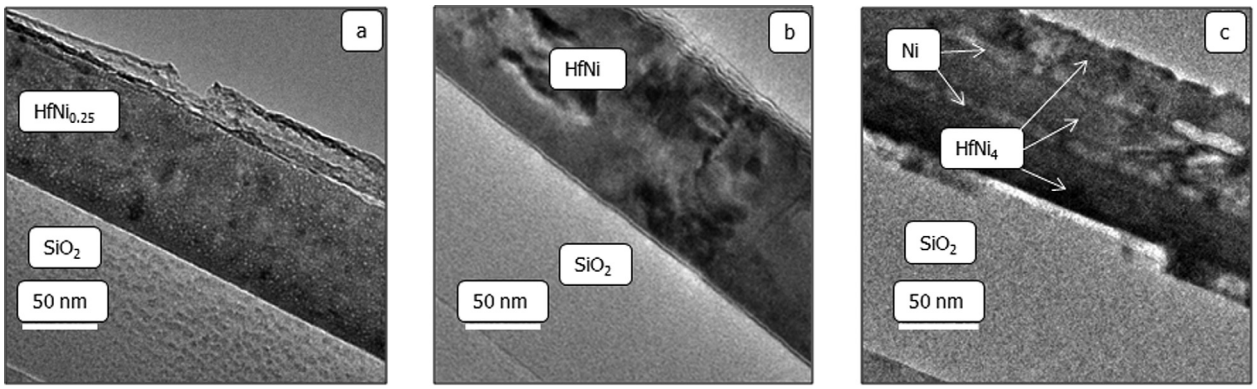

FIG. 3. Cross-section TEM micrograph of multilayer samples after thermal treatment. The nominal Ni concentrations of the samples are (a) 20 at. % Ni, (b) 50 at. % Ni, and (c) 80 at. % Ni.

where K_{SiO_2} is the dielectric constant of SiO_2, ε_0 is the vacuum permittivity, A is the area of the capacitor, and EOT is the equivalent oxide thickness, which is defined as $EOT = {}^{K_{SiO_2}}/_{K_{di}} t_{di}$, where K_{di} and t_{di} are the effective dielectric constant and the physical thickness of the gate dielectric. Since a decrease in the dielectric constant of SiO_2 due to some diffusion is highly improbable, the capacitance decrease is either due to a lower effective area or a higher oxide thickness. The latter possibility can be explained by some chemical reaction between the metal and the oxide. However, there is no evidence for an additional oxide layer in TEM micrographs. Furthermore, an additional oxide layer should not depend on the initial thicknesses of the oxide stacks, while our results show that the difference in EOT between the as-deposited samples and the thermally treated samples is directly proportional to the initial EOT of the stack.

The possibility of a lower effective area can be explained by the formation of Kirkendall voids, which has been previously observed in similar metallic systems.[33–36] In those systems, which is similar to our Hf/Ni stack exhibit solid state amorphization and have one dominant diffusing species, the voids are formed in the side of the dominant diffusing element. In our system, the diffusion flux of Ni is larger than the diffusion flux of Hf. Therefore, if the Ni layer does not entirely diffuse and "disappears" altogether into the $HfNi_x$ layer, then the voids should be formed somewhere at the innermost part of the Ni layer. Consequently, the effective capacitance area of the "Ni-under" samples should be smaller than the area before the thermal treatment, according to Eq. (1). A cross-section TEM sample was prepared from a Ni/Hf(20 nm)/Ni(50 nm)/SiO_2 capacitor and the micrograph is shown in Fig. 6. Two clear phenomena are observed in this micrograph. One phenomenon is that the thickness of

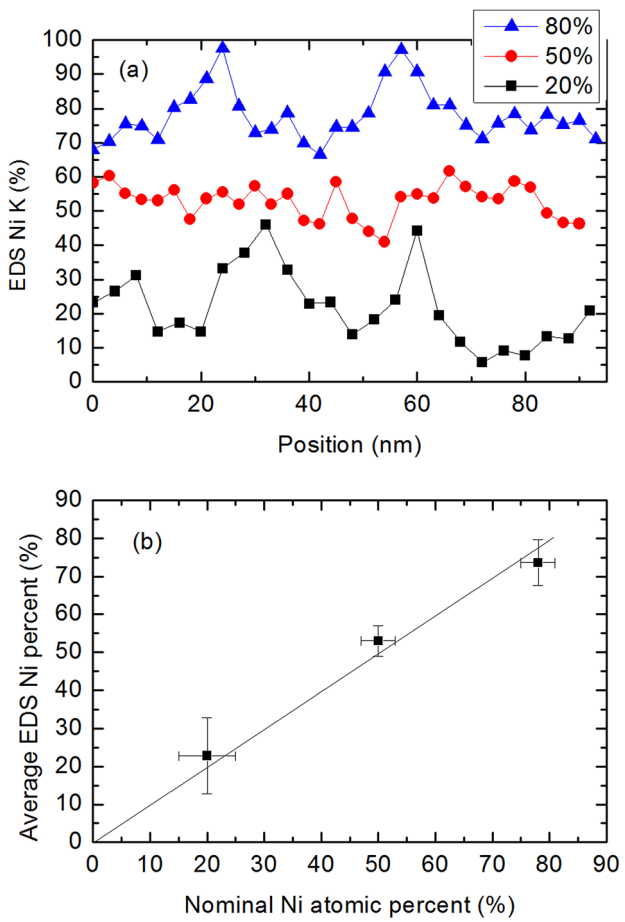

FIG. 4. (a) EDS line profile of Ni for the samples shown in Fig. 3. (b) The average EDS counts of Ni in the $HfNi_x$ layer vs. the nominal Ni concentration.

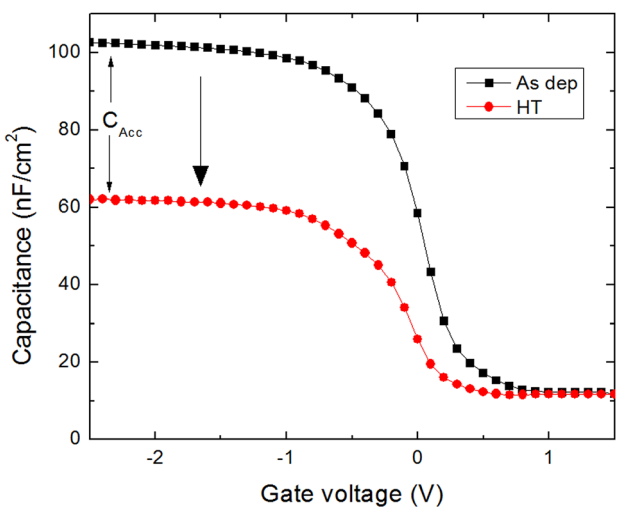

FIG. 5. C-V measurement before and after a heat treatment of 400 °C of a Ni/Hf(35 nm)/Ni(35 nm)/SiO_2 sample.

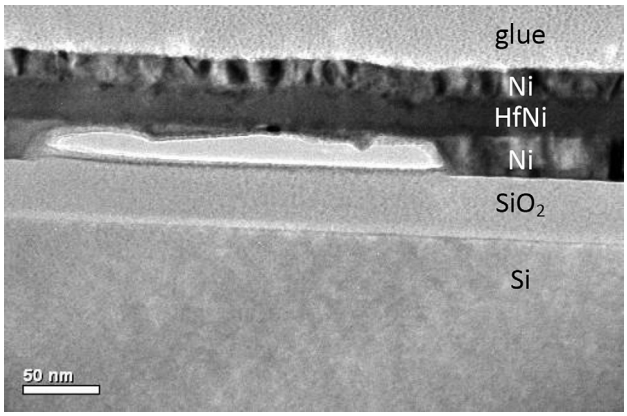

FIG. 6. Cross-section TEM micrograph of a Ni/Hf(20 nm)/Ni(50 nm)/SiO_2 capacitor after a 400 °C heat treatment.

the $HfNi_x$ amorphous layer is larger than the initial Hf layer, due to the incorporation of Ni atoms. The other phenomenon is the formation of a Kirkendall void, which extends over the entire thickness of the Ni layer.

Another set of experiments has been carried out in order to track the formation of the voids by heating cross-sectional samples *in situ* in the TEM up to 490 °C. Theses samples have been especially prepared for the heating experiment as explained in Sec. II. The TEM micrograph in Fig. 7(a) shows the stack before heating. The order of the stack is Pt(C)/Ni/Hf/SiO_2, where the amorphous Pt(C) is deposited as a protection layer as a part of the procedure of the cross-sectional TEM sample preparation. Figure 7(b) shows the initial stage of void formation in the Ni at the Pt(C)/Ni interface. Figures 7(c) and 7(d) show the stack at 490 °C after 12 and 77 min, respectively. We observe a size increase of the void and a thickness increase of the Hf layer with time. A complementary experiment was performed using EFTEM. An elemental map of Ni at the same temperature was measured *in situ* using the Ni-$L_{2,3}$ edge. The stack before and after heating is shown in Figs. 8(a) and 8(b), respectively. The elemental

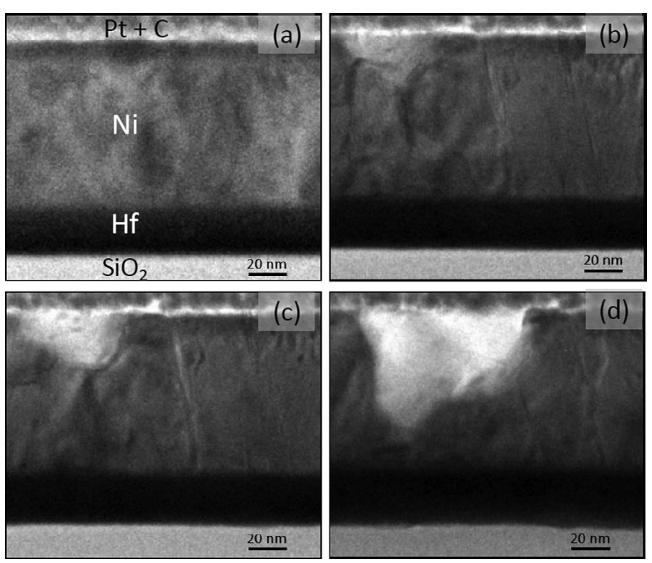

FIG. 7. Cross-section TEM micrographs of an *in situ* heating experiment done on a Ni(91 nm)/Hf(28 nm)/SiO_2 stack. (a) Before heating. (b) At 490 °C, the voids immediately appear. (c) and (d) are 12 and 77 min after (b).

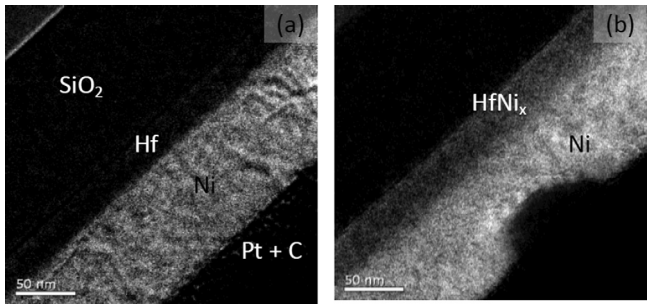

FIG. 8. EFTEM elemental map of Ni $L_{2,3}$-edge of the Ni(91 nm)/Hf(28 nm)/SiO_2 stack before heating and at 490 °C after 30 min.

maps show that the Ni atoms diffuse into the Hf layer uniformly regardless of the distance from the void.

Assuming that only the area of the capacitor changes between the AD samples and the heat treated (HT) samples, and also that the voids contribution to the total capacitance is negligible due to their large length in the dimension perpendicular to the interface (which is approximately equal to the entire initial thickness of the Ni layer, as shown in Fig. 6), the C_{Acc} equation can be derived into

$$C_{Acc,HT} = \frac{A_{HT}}{A_{AD}} C_{Acc,AD}. \quad (2)$$

Capacitors with several different dielectric thicknesses have been used for C-V measurements, enabling to draw a $C_{Acc,HT}$ vs. $C_{Acc,AD}$ plot, as shown in Fig. 9 for the Ni/Hf(20 nm)/Ni(50 nm)/HfO_2 sample. The linear fit of the data clearly deviates from the $C_{Acc,HT} = C_{Acc,AD}$ line and the slope of this line yields the A_{AD}/A_{HT} ratio. This ratio can provide an accurate estimate of the void concentration. The results of the A_{HT}/A_{AD} ratio for the other samples extracted using Eq. (2) are summarized in Table I. In addition, the intercept at the axis proves that the voids contribution to capacitance is indeed negligible.

The table shows that there is an increase in the total area of the Kirkendall voids adjacent to the substrate oxide as the initial Ni/Hf thickness ratio decreases, just as expected for

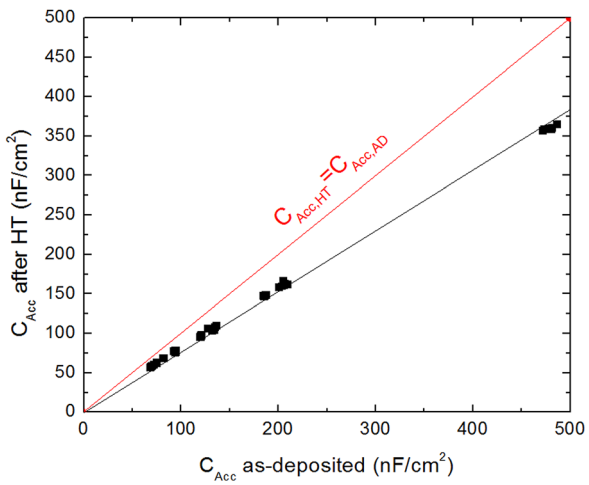

FIG. 9. C_{Acc} of Ni/Hf(20 nm)/Ni(50 nm)/HfO_2 samples after heat treatment vs. C_{Acc} of the same samples before heat treatment.

TABLE I. A_{HT}/A_{AD} of capacitors with different initial Hf/Ni thicknesses on SiO_2 and HfO_2.

	Hf(20)/Ni(50) /SiO_2	Hf(20)/Ni(50) /HfO_2	Hf(35) /Ni(35)/SiO_2	Hf(35)/Ni(35) /HfO_2
A_{HT}/A_{AD}	0.79 ± 0.1	0.77 ± 0.1	0.56 ± 0.1	0.5 ± 0.2

this kind of a system.[29] The area of the voids is also invariant of the substrate oxide (i.e., SiO_2 or HfO_2). It is important to note that no significant decrease in capacitance is observed for the "Ni-under" samples with a 10 nm thick Ni layer. However, cross-section TEM micrographs of samples taken from such capacitors shows that Kirkendall voids are formed in these samples as well, but to a much lesser extent. The remaining Ni layer is very thin and the voids are filled with SiO_2. Figure 10 shows the TEM micrograph of a Ni/Hf(10 nm)/Ni(10 nm)/SiO_2 sample and EDS line profiles made at two different points along the metal stack/SiO_2 interface. Two different interfaces can be observed along the oxide: an $HfNi_x/SiO_2$ interface for the line profile incident to a void and a Ni/SiO_2 interface for the line profile incident to an area between voids.

C. Capacitance increase in "Hf-under" samples

A substantial increase in the C_{Acc} with respect to the as-deposited samples is observed in "Hf-under" samples after heat treatment. This increase in C_{Acc} is observed both on SiO_2 and on HfO_2. It is assumed to be associated with the "scavenging" phenomenon which has been previously observed for high-K stacks with pure reactive metals.[37–40] In these systems, Si-O bonds in the SiO_2 layer are broken and O atoms diffuse through the oxide stack into the gate metal, which can absorb a large concentration of O atoms while sustaining its conducting properties.[38] The dissociated Si atoms are believed to grow epitaxially on the Si substrate without introducing additional mid-gap states into the SiO_2/Si interface.[39] Our C-V measurements indeed indicate that no substantial increase in such states takes place, as the slope in the depletion region does not change. This phenomenon was also observed by Lee *et al.* when they used Hf as a bottom electrode beneath the Ni layer.[14]

Assuming that the thinning of the SiO_2 layer does not depend on the thickness of the layer, the dielectric capacitance of the as-deposited sample can be expressed as two capacitors in series consisting of the capacitance of the sample after heat treatment and the scavenged capacitance C_{Get}

$$\frac{1}{C_{Acc,AD}} = \frac{1}{C_{Acc,HT}} + \frac{1}{C_{Get}}. \tag{3}$$

This can be written also

$$\frac{1}{C_{Acc,HT}} = \frac{1}{C_{Acc,AD}} - \frac{1}{C_{Get}}. \tag{4}$$

Using Eq. (4) for a series of different dielectric thicknesses, the thickness of the scavenged SiO_2 can be extracted from the intercept of a $1/C_{Acc,HT}$ vs. $1/C_{Acc,AD}$ plot. In Fig. 11, we show such a plot for the Ni(10 nm)/Hf(90 nm)/HfO_2 samples. A linear fit of the data shows that the slope is 1 like the $1/C_{Acc,HT} = 1/C_{Acc,AD}$ line while there is a constant offset between the two lines. The oxides of the samples after heat treatment are constantly thinner than the as deposited samples by 2.6 ± 0.2 nm. The phenomenon is hardly noticeable for capacitors with an Hf layer thinner than 5 nm. Above 10 nm it is substantial, but no correlation was found between the initial Hf thickness and the magnitude of the "scavenging." This probably indicates that other parameters, such as the initial O concentration in Hf, have a significant influence on the reaction as well.

The "scavenging" reaction has been previously reported only for pure metals. In our case, it is not determined whether the $HfNi_x$ alloy itself takes part in this reaction. If $HfNi_x$ can cause the "scavenging" reaction, then its reaction

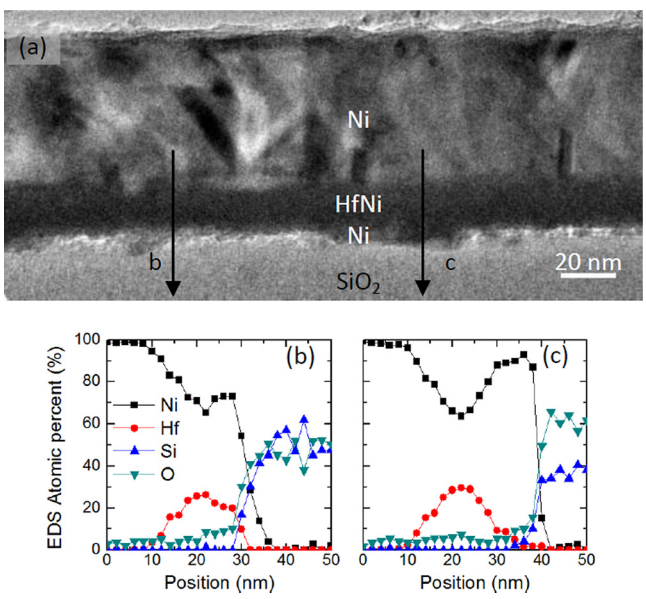

FIG. 10. (a) Cross-section TEM micrograph from a Ni/Hf(10 nm)/Ni(10 nm)/SiO_2 capacitor after a heat treatment of 400 °C. 2 EDS line profiles were performed incident to: (b) Voids. (c) Area between voids.

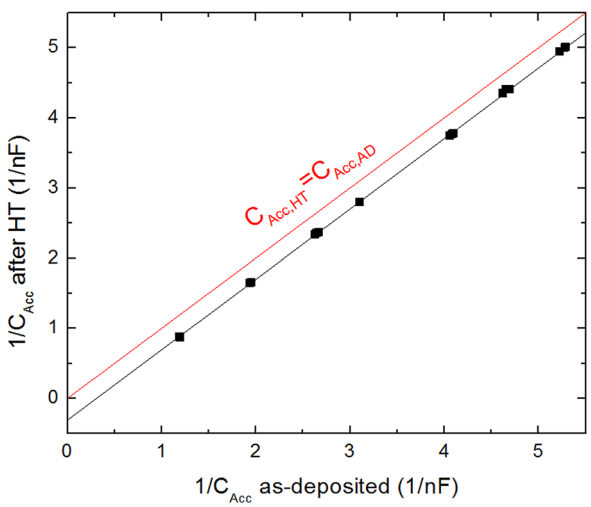

FIG. 11. $1/C_{acc}$ of Ni(10 nm)/Hf(90 nm)/HfO_2 samples after heat treatment vs. $1/C_{acc}$ of the same samples before heat treatment.

rate is independent of the Ni diffusion rate. However, if the formation of $HfNi_x$ inhibits the reaction, then the "scavenging" reaction must be faster than the diffusion of Ni into Hf in order for the reaction to take place.

An abrupt interface between Si and HfO_2 is attainable when employing the "Hf-under" approach for intermixing. However, in samples with a thin initial SiO_2 thickness a massive reaction between Si and Ni was observed in the Si side of the oxide stack, probably due to the fact that the SiO_2, which acts as a diffusion barrier between Ni and Si, is eliminated.

D. Work-function dependence on composition

The Φ_M^{Eff} values of the $HfNi_x/SiO_2$ capacitors are extracted using the following:[41]

$$V_{FB} = \Phi_M^{Eff} - \Phi_S - \frac{Q_{SiO_2/Si} EOT}{\varepsilon_{SiO_2}}, \quad (5)$$

where V_{FB} is the flatband voltage, Φ_S is the semiconductor substrate work-function, $Q_{SiO_2/Si}$ is the planar charge density at the SiO_2/Si interface, ε_{SiO_2} is the permittivity of SiO_2, and *EOT* is the equivalent oxide thickness. V_{FB} and *EOT*are extracted from the C-V measurements curves, which are done for all different capacitors at different EOT values. The Φ_M^{Eff} values are extracted from the intercept of the linear fits of V_{FB} vs. *EOT* plots according to Eq. (5).

The Ni thickness ratio (R_{Ni}) in the "Hf-under" samples is defined as the ratio between the thickness of the Ni layer (t_{Ni}) and the sum of the thickness of the Hf layer (t_{Hf}) and t_{Ni} as $R_{Ni} = t_{Ni}/(t_{Ni} + t_{Hf})$, illustrated in Fig. 12(a). The Φ_M^{Eff} values as a function of the R_{Ni} for the "Hf-under" capacitors are marked in Fig. 12(c) by rectangles. The pure Hf point ($R_{Ni} = 0$) refers to the Ni/Hf capacitors that were subjected to a 300 °C anneal, as explained in the Sec. II. In the two samples with t_{Ni} ratio >0.67, which corresponds to an atomic percentage of ~78 at. % Ni, only part of the Ni top layer diffuses into the Hf layer and the excess Ni remains as a top layer. Therefore, the actual Ni concentration in the bottom layer is approximately ~78 at. % Ni, invariant of the R_{Ni} value. The other two samples undergo full intermixing after the thermal treatment. Figure 12(c) clearly shows that for the "Hf-under" configuration there is a large difference between the Φ_M^{Eff} values of pure Hf and pure Ni and also that the Φ_M^{Eff} values of the alloys are all very close to the Φ_M^{Eff} value of pure Hf.

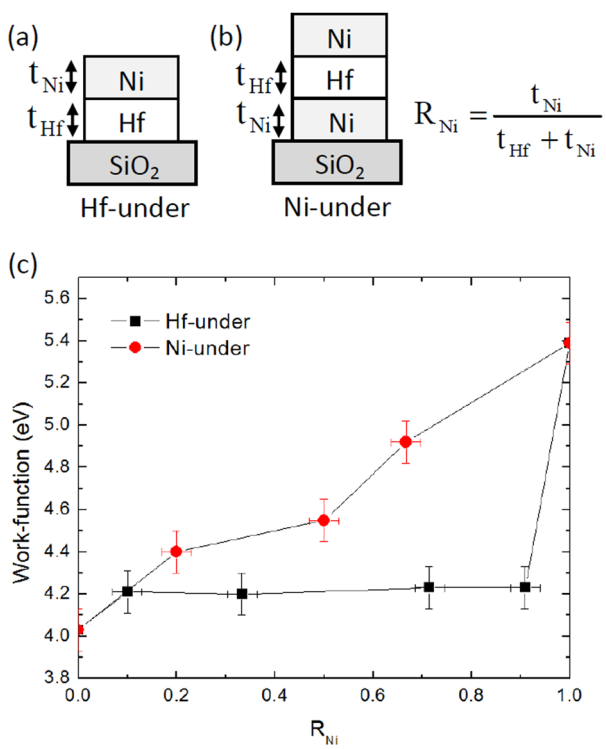

FIG. 12. Effective work-function vs. Hf thickness ratio for "Hf-under" and "Ni-under" capacitors.

The results of the Φ_M^{Eff} measurements for the "Ni-under" capacitors are marked in Fig. 12(c) by circles. The R_{Ni} value for these samples is the ratio between the bottom Ni layer thickness and the sum of thicknesses of the bottom Ni layer and the intermediate Hf layer, as illustrated in Fig. 12(b), assuming that Ni atoms from the top Ni layer do not diffuse into Hf at 400 °C. The results shown are for capacitors with a bottom Ni layer of $t_{Ni} = 10$ nm and various Hf layer thicknesses, since these capacitors do not exhibit the above discussed decrease in capacitance. There is a clear trend of Φ_M^{Eff} increase as the intermediate Hf layer in the stack becomes thinner (R_{Ni} increase).

The Φ_M^{Eff} values of the $HfNi_x/HfO_2$ capacitors are extracted using:[42]

$$V_{FB} = \Phi_M^{Eff} - \Phi_S - \frac{Q_{HfO_2/SiO_2} EOT_{HfO_2}}{\varepsilon_{SiO_2}} - \frac{Q_{SiO_2/Si} EOT}{\varepsilon_{SiO_2}}, \quad (6)$$

where Q_{HfO_2/SiO_2} is the planar charge density at the HfO_2/SiO_2 interface, *EOT* is the equivalent oxide thickness of the entire oxide stack, and EOT_{HfO_2} is the equivalent oxide thickness of only the HfO_2 layer. The dielectric constant of the HfO_2 used in these samples has been measured to be $K = 22 \pm 1$.[43] Since the physical thickness of the HfO_2 layer is 4 nm, the EOT is approximately 0.7 nm. No shift greater than 0.1 eV is expected to be measured in V_{FB} for any Q_{HfO_2/SiO_2} smaller than 3×10^{12} cm^{-2}, which is an extremely high charge density. Therefore, the error in the Φ_M^{Eff} value is assumed to be of the order of 0.1 eV. The V_{FB} vs. *EOT* plots of the HfO_2 samples are shown in Fig. 13, clearly exhibiting linear behavior in accordance with Eq. (6).

Figure 14 shows the Φ_M^{Eff} compositional dependence of both the $HfNi_x/SiO_2$ and $HfNi_x/HfO_2$ capacitors. In the case of the "Hf-under" samples (marked in black squares), the compositions of the alloys are calculated straightforwardly from the R_{Ni} and the density of both elements. The interfaces of the "Ni-under" samples (in black circles) with the oxides contain either voids or two phases, as explained in Sec. II of the results and therefore need more careful analysis, which is elaborated on later in this chapter. The experimental data points are connected with a straight line in order to show the trend.

The results of the KP measurements are also shown in Fig. 14, where the values of the Ni concentrations are based

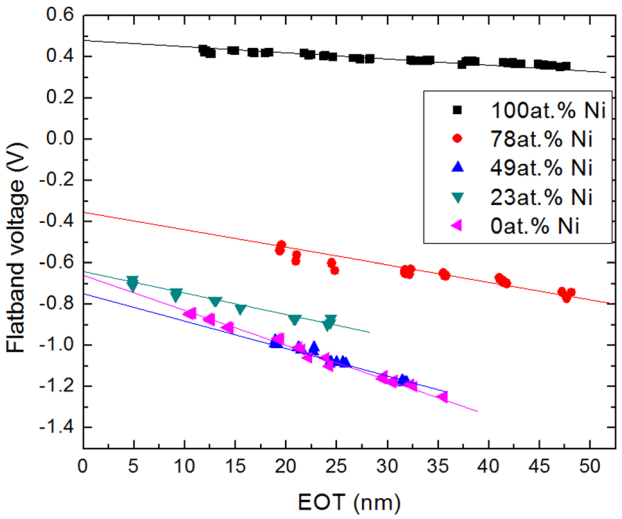

FIG. 13. Flatband voltage vs. EOT plots of several $HfNi_x/HfO_2$ samples.

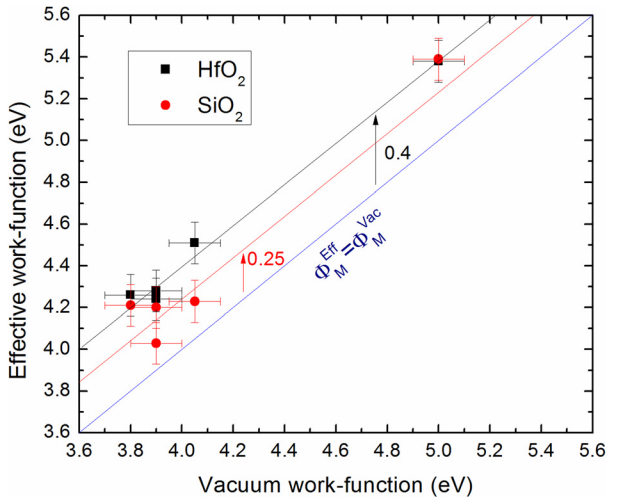

FIG. 15. Effective work-function values of $HfNi_x/SiO_2$ and $HfNi_x/HfO_2$ systems vs. vacuum work-function values.

on a uniform distribution in composition of the samples. The pure Hf Φ_M^{Vac} value from the literature is taken as a reference for the KP results0.[21] The compositions between 78 and 100 at. % Ni cannot be reached since the $Ni/HfNi_x$ interface is meta-stable at these temperatures, inhibiting Ni diffusion. In the three systems with pure $HfNi_x$ at the interface/surface, there is a similar compositional dependence, where all $HfNi_x$ compositions have work-function values similar to the work-function value of pure Hf. A few compositions even have a work-function lower than that of pure Hf. In other words, the Fermi level position of the Hf-Ni alloy system is pinned to that of pure Hf. These results are also in accordance with the results of Lee *et al.*[14]

A comparison between the Φ_M^{Vac} values of the alloy and the Φ_M^{Eff} values on both oxides is shown in Fig. 15. Both lines are parallel to the $\Phi_M^{Eff} = \Phi_M^{Vac}$ line but the $Hf\text{-}Ni/SiO_2$ Φ_M^{Eff} vs. Φ_M^{Vac} line and the $Hf\text{-}Ni/HfO_2$ Φ_M^{Eff} vs. Φ_M^{Vac} line are shifted by about 0.25 eV and 0.4 eV above the $\Phi_M^{Eff} = \Phi_M^{Vac}$ line, respectively. The magnitude of the shift can also be

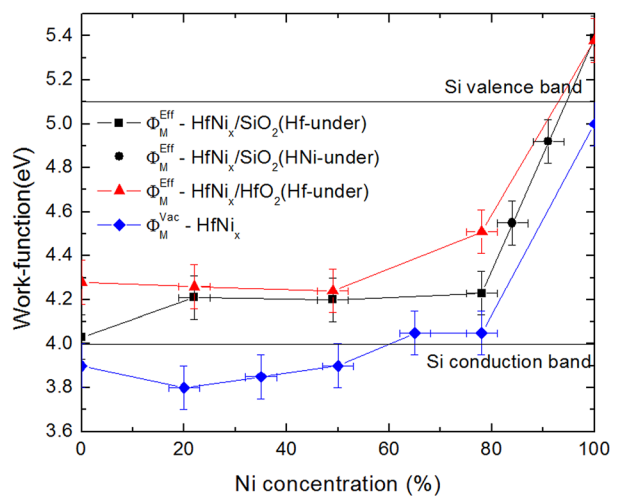

FIG. 14. Effective work-function compositional dependence of $HfNi_x/SiO_2$ and $HfNi_x/HfO_2$ and the vacuum work-function compositional dependence on $HfNi_x$ as measured by KP. The experimental data points are connected with a straight line in order to guide the eye.

caused by the selected reference for the KP measurements. Choosing the Ni Φ_M^{Vac} value from the literature as the reference of the measurement instead of the Hf Φ_M^{Vac} value would reduce the shift to 0.2 eV for the Φ_M^{Eff} on HfO_2 and 0.05 eV for the Φ_M^{Eff} on SiO_2, which is within the experimental error.

This correlation between Φ_M^{Eff} and Φ_M^{Vac} indicates that the Fermi level pinning cannot be attributed to the dielectric material. In such a case, the Φ_M^{Eff} values would have converged towards a certain value, while the results show that pure Ni has a Φ_M^{Eff} value very different than that of pure Hf and the alloys.[27,28] Furthermore, the Fermi level pinning of the alloys appears also in vacuum. The shift from the $\Phi_M^{Eff} = \Phi_M^{Vac}$ line could be indicative of either a large density of trapped charges in the HfO_2 layer or a constant dipole layer in the stack which causes band bending.[44–46]

The similarity in compositional dependence between the $HfNi_x/SiO_2$ and $HfNi_x/HfO_2$ capacitors could indicate that the $HfNi_x$/oxide interface is Hf-rich. In other words, the interfacial composition is nearly invariant to the bulk $HfNi_x$ composition, effectively pinning all the Φ_M^{Eff} values to that of Hf. A significant driving force for this phase boundary Hf enrichment phenomenon might be the large affinity to oxygen, which is abundant in the underlying oxide layer.

The pinning of the $HfNi_x$ Φ_M^{Vac} values to that of Hf can similarly be associated with Hf enrichment at the surface of the amorphous alloys. This assumption is supported by previous studies on binary alloys which have shown a similar Φ_M^{Vac} compositional dependence. Several binary metallic systems (Ag-Au,[47,48] Ag-Pd,[49,50] Cu-Ni,[51–56] and Au-Pt (Ref. 57)) which had been studied for both their Φ_M^{Vac} and segregation compositional dependence have shown a clear correlation between the segregation of the low Φ_M^{Vac} metal to the surface of the alloy and the non-linearity of the Φ_M^{Vac} compositional dependence, i.e., a pinning of Φ_M^{Vac} values to that of the lower-Φ_M^{Vac} metal. In the Cu-Ni and Au-Pt systems, the Φ_M^{Vac} values at some compositions were even lower than the Φ_M^{Vac} value of the lower Φ_M^{Vac} metal. The correlation between

surface composition and Φ_M^{Vac} in these binary alloy systems had previously been studied theoretically.[58] Also, experimental studies have shown that the work-function of metals can be significantly altered due to segregation even at low contents in the Cu-Ti system.[59,60]

Furthermore, theoretical studies have shown that the atomic concentration of the surface layer has the most significant effect on the work-function value in the Al-Ni, Al-Pt, Mo-W, Nb-W, Ni-Pt, and Mo-Ta alloy systems as well as in the case of several elements adsorbed on the surface of W.[61–67]

Regarding the feasibility of the Hf enrichment in the $HfNi_x$ system, it has been experimentally observed that the surface energy (γ) of Hf is lower than that of Ni.[68] This can be explained by the high affinity of Hf to O atoms, namely its tendency to oxidize.[69] The presence of excess Hf at the surface in the $HfNi_x$ amorphous solution is thus explained by its effect on lowering the surface energy. For example, it is known that Hf is incorporated in low concentrations into Ni-based alloys for adhesion enhancement,[70] which is an indication of surface enrichment by Hf. We assume that the enrichment of the $HfNi_x$ surface with Hf atoms occurs rapidly since there is no difference between Φ_M^{Vac} measurements before and after heating in the KP chamber.

However, there has been thus far no experimental evidence in the literature of equilibrium segregation of Hf in Ni despite broad attempts to do so, which is probably an indication that the "true" surface energy of Hf is not lower than that of Ni. The γ values found in the literature are actually lower than the equilibrium values most probably because Hf oxidizes rapidly at high temperatures. Since our KP chamber was in high vacuum but not in ultra-high vacuum, one cannot exclude the presence of oxygen in the ambient of the $HfNi_x$ solution. In other words, our system is closer to the conditions reported in the literature than to equilibrium. For example, using reported γ values in the models presented in Ref. 52 the expected Φ_M^{Vac} value of the 78 at. % Ni is 4 eV with the image force model and 4.3 eV with the simple surface mixture model.

Alas, we have no direct experimental evidence that the surface contains more Hf atoms than the bulk. The amorphous structure of the films along with the fact that even small compositional changes in one atomic layer is sufficient to induce large Φ_M^{Vac} shifts mean that such an experimental attempt is quite challenging. Such a future work is encouraged by the authors of this paper. Our main claim is that the pinning of the Φ_M^{Vac} values to that of pure Hf is an indication of Hf enrichment at the surface.

Since the $HfNi_x$ alloys with compositions between 0 and 40 at. % Ni contain a certain amount of Hf_2Ni, its effect on the work-function should also be considered. In order to evaluate the Φ_M^{Vac} value of Hf_2Ni, first-principles calculations (at 0 K) are performed for the Hf_2Ni (tetragonal) intermetallic compound, as well as for pure Ni (f.c.c.) and Hf (h.c.p.) crystals, based on the density functional theory (DFT),[71–73] employing the Vienna *ab initio* simulation package (VASP).[74–76] The preliminary calculations of the Φ_M^{Vac} values for pure Ni and pure Hf are done in order to establish a theoretical baseline. The general gradient approximation (GGA) functional is utilized to express the exchange correlation energy and the projector augmented wave (PAW) potentials to handle the core electrons density.[77] A plane-wave basis set is used having an energy cut-off ranging between 270 and 400 eV, depending on the material, to represent the Kohn-Sham wave functions0.[78] In order to sample the Brillouin zone and obtain energy convergence, a uniform Monkhorst-Pack *k*-point mesh with densities ranging between 0.1 and 0.5 $Å^{-1}$ is selected, depending on the material.

Prior to Φ_M^{Vac} calculations, the bulk Ni, Hf, and Hf_2Ni structures are relaxed by minimizing their total energies using a threshold of 20 meV $Å^{-1}$ Hellman-Feynman force.[79] The lattice parameters of the above structures are calculated to be a = 3.5239 Å for Ni, a = 3.19878 and c = 5.05858 Å for Hf, and a = 6.41684 and c = 5.22841 Å for Hf_2Ni, in agreement with experimental room temperature values.[80–82] Based on the above relaxed structures, the surfaces are constructed with different orientations in the configuration of repeating units comprising slab + vacuum, where the size of slabs is set to be 4 periodic structural units. Each structural unit is equivalent to 2–4 atomic layers depending on the orientation, and the vacuum layer thickness is determined to be 10 Å. These magnitudes are optimized to yield convergent total energies.[83,84] Figure 16 shows an example for such a slab + vacuum construction.

The Φ_M^{Vac} values are calculated based on the surface-averaged electronic local potential and that one of the bulk,[85] by optimizing the total energies of the slabs, employing an energy threshold of 10^{-5} eV per atom for convergence.

In addition to Φ_M^{Vac} values, the energies of several low-index Ni-, Hf-, and Hf_2Ni-surfaces are calculated to estimate the preferred surface orientation. To this end, the total molar

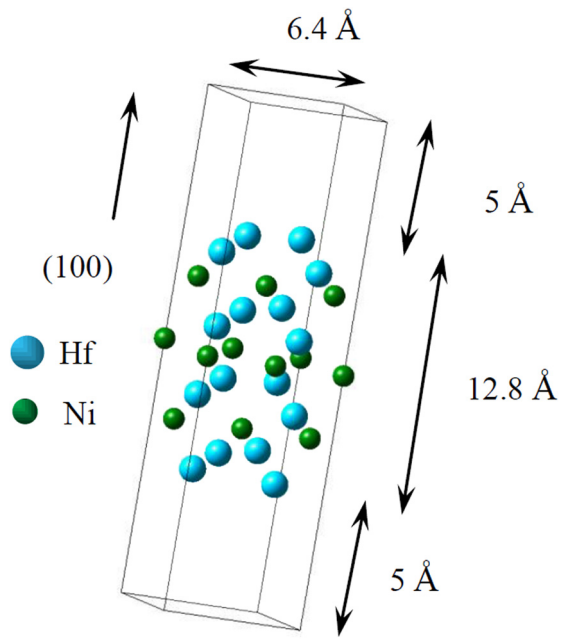

FIG. 16. An example of a symmetric $6.4 \times 6.4 \times 22.8$ $Å^3$, (100)-oriented Hf_2Ni slab model with Hf terminating planes, consisting of two repeating structural units along the [100]-direction with a total thickness of 12.8 Å and a vacuum region having 10 Å thickness. Ni atoms are marked in green, and Hf atoms are marked in aqua.

energies of the above slab models, E_{slab}, and of the bulk materials, E_{bulk}, are calculated and the surface energy is expressed as follows:[85]

$$\gamma = \frac{n}{2A}(E_{slab} - E_{bulk}), \tag{7}$$

where n is the number of moles in the a slab and A is the surface area.

First, the effect of surface relaxation on the calculation of the Φ_M^{Vac} and γ values is examined. Disregarding surface relaxation, the calculated surface energy value of the Hf (001) is 1.82 J/m^2, whereas a value of 1.71 J/m^2 is obtained considering surface relaxation in our calculations; the difference between both values is insignificant. The Φ_M^{Vac} value is not considerably affected by surface relaxation either, and varies from 4.375 to 4.329 eV. Therefore, we do not consider surface relaxation further in our calculations.

Our calculations are in agreement with those of Skriver and Rosengaard regarding the γ values for both Ni(FCC-111) and Hf(FCC-111).[86] However, the linear Muffin-Tin orbitals approximation (LMTO) method applied by Skriver and Rosengaard constantly overestimates the Φ_M^{Vac} values of transition metals. The reason for this is that while LMTO is computationally easier than our VASP calculations (in terms of high power computing), it has been developed for systems in which electrons are more localized (tightly bound) such as molecules and even closely packed solids. On the other hand, the VASP calculations employ a planar wavefunctions basis set, which is better for most crystals.

Table II displays the calculated Φ_M^{Vac} values of several selected Ni, Hf, and Hf_2Ni surfaces. For the latter, both Ni and Hf terminating planes are considered. The surface energies for the corresponding Ni and Hf surfaces are presented in Table II as well.

Based on the data in Table II, the preferred surface orientations (those with the lowest γ) of Ni and Hf are (111) and (001), respectively, as expected for f.c.c. and h.c.p. structures. The corresponding Φ_M^{Vac} values are 5.198 and 4.375 eV for Ni (111) and Hf (001), respectively. For Hf_2Ni, in general, the Φ_M^{Vac} values obtained for Ni terminations are considerably larger with respect to the Hf termination, in accordance with the trend for these pure metals. The Hf_2Ni termination plane with the lowest γ value is the Ni(100) plane with a Φ_M^{Vac} value of 3.993 eV. The Φ_M^{Vac} values of Hf, Hf_2Ni, and Ni are 3.6 ± 0.6 eV, 3.8 ± 0.3 eV, and 4.9 ± 0.3 eV, respectively, as an average on all calculated terminating planes. The Φ_M^{Vac} values of Hf and Hf_2Ni are close and significantly lower than the Φ_M^{Vac} value of pure Ni, in accordance to the experimental results. Similar DFT results have been previously reported for the Al-Cu system, where the values of the Al_2Cu and Al_3Cu_2 phases are even lower than the values of both pure Al and pure Cu.[87] To summarize the DFT results, they show that the presence of the Hf_2Ni phase also has a part in the pinning of the work-function values.

TABLE II. Φ_M^{Vac} and γ values calculated using DFT.

Crystal	surface	Terminating plane	Φ_M^{Vac} (eV)	γ (J/m^2)
Ni	(100)	…	5.012	2.95
	(110)	…	4.637	2.84
	(111)	…	5.198	2.65
Hf	(001)	…	4.375	1.82
	(100)	…	3.77	1.86
	(110)	…	3.045	1.95
	(111)	…	3.323	2.09
Hf_2Ni	(100)	Hf	3.599	2.25
	(100)	Ni	3.993	1.84
	(001)	Hf	3.753	2.04
	(001)	Ni	4.385	2.09
	(110)	Hf	3.439	2.52
	(110)	Ni	4.035	1.87
	(101)	Hf	3.657	1.92
	(101)	Ni	3.812	2.40
	(111)	Hf	3.740	2.10
	(111)	Ni	3.953	2.07

It should be noted that the Fermi level positions of the "Ni"-under capacitors are not pinned to that of pure Hf as shown in Fig. 12. The reason for this is the dual phase, which is formed across the electrode/oxide interface oxides as explained in Sec. II. The dual-phase consists of a Ni/SiO_2 interface and an $HfNi_x/SiO_2$ interface like the one shown in Fig. 10. The Ni concentration of the dual-phase interfaces can then be calculated by estimating X_{HfNi}, the areal ratio between the Ni/SiO_2 interface and $HfNi_x/SiO_2$ interface, using the rule of mixture

$$\Phi_{HfNi/Ni} = X_{HfNi}\Phi_{HfNi} + (1 - X_{HfNi})\Phi_{Ni}, \tag{8}$$

where $\Phi_{HfNi/Ni}$ is the measured Φ_M^{Eff} of the dual phase capacitors, Φ_{HfNi} is the measured Φ_M^{Eff} of the solution with 78 at. % Ni, and Φ_{Ni} is the measured work-function of pure Ni. Substituting 4.55 eV, 4.2 eV, and 5.4 eV, respectively, for the Ni/Hf(10 nm)/Ni(10 nm) samples yields $X_{HfNi} = 0.71$ and using the lever rule the composition is ~84 at. % Ni. Similarly, substituting $\Phi_{HfNi/Ni} = 4.92$ eV for the Ni/Hf(5 nm)/Ni (10 nm) samples yields $X_{HfNi} = 0.4$ and a composition of ~91 at. % Ni. The concentration of the $HfNi_x/SiO_2$ interface is larger for the sample with the thicker initial Hf layer, as predicted for the Kirkendall voids mechanism.

The result of the dual-phase interface is a steep increase in Φ_M^{Eff} from the value for the 78 at. % Ni amorphous solution to that of pure Ni. The significance of this is that tuning the Φ_M^{Eff} of Hf-Ni gates is possible with even small variations in composition. However, the formation of the dual-phase alloys is accompanied by a roughening of the interface which degrades the electrical quality of the device. Therefore, a different method of fabrication, namely co-deposition of the metals, might prove to be better for technological applications.

IV. CONCLUSIONS

The Hf-Ni system is a promising alloy system to be used as gate metal for future CMOS technology devices. The dominant diffusant in this system is Ni, causing an intermixing of both components, which results in a uniform amorphous layer with a composition in the range of 40-78 at. %

Ni, depending on the initial layer thicknesses, after thermal treatments of up to 500 °C. The order of the metals in the stack has a major importance on the properties. On one hand, the "Ni-under" MOS capacitors exhibit a decrease in capacitance, which is attributed to the formation of Kirkendall voids. Although no significant decrease in capacitance is observed in samples with a thin Ni layer, the voids are observed by TEM. On the other hand, the "Hf-under" MOS capacitors exhibit an increase in capacitance, which is attributed to the scavenging ability of pure Hf, and would seem to be highly beneficial for further scaling of devices. However, in order to use the Hf-Ni system as gate metal, the silicidation phenomenon should be avoided. This could be done by limiting the initial Ni thickness and thereby avoiding the diffusion past the Hf layer. A thicker initial layer of Hf or Ni can also inhibits the Ni diffusion towards the Si.

The compositional dependence of Φ_M^{Eff} on SiO_2 and HfO_2 is experimentally measured and compared with the compositional dependence of Φ_M^{Vac}. All compositions under 78 at. % Ni exhibit a Fermi level pinning to the Fermi level position of pure Hf. This behavior is attributed to Hf enrichment at the solid solution surface (or the metal/oxide interface). The presence of the Hf_2Ni intermetallic phase at the 0–40 at. % Ni compositions does not alter this trend due to its low Φ_M^{Vac} value. However, "Ni-first" capacitors with initial metal stacks that consist of a thin Ni layer exhibit Φ_M^{Eff} values closer to that of pure Ni, enabling to tune the Φ_M^{Eff} values over a range of approximately 1 eV. The metal/oxide interface of these capacitors is a dual phase consisting of Ni/oxide and $HfNi_x$/oxide interfaces that function as parallel capacitors. The Φ_M^{Eff} values of the alloy system on HfO_2 are about 0.2 eV–0.4 eV above the Φ_M^{Vac} values, a shift which is attributed to band bending due to charges in the HfO_2 layer or to dipoles in the oxide stack. The disadvantages exhibited by the Hf-Ni alloy system for incorporation as gate electrode in MOS devices can be overcome if it would be fabricated using a co-deposition technique rather than by multi-layer deposition.

ACKNOWLEDGMENTS

We acknowledge the support of ALPHA consortium (Israel Ministry of Industry and Trade) and the Russell Berrie Nanotechnology Institute at Technion. We thank C. Cytermann from the Solid State Institute for ToF-SIMS measurements, Dr. B. Meyler from the Microelectronics Research Center for the HfO_2 deposition, and A. Shai from the Microelectronics Research Center for support with the e-gun evaporation. We thank Dr. T. Cohen-Hyams for the preparation of the TEM samples using FIB and to R. Winter for the preparation of the conventional TEM samples. We thank Y. Moses for constructing the *in situ* KP chamber and Dr. G. Frant for operating the sputtering chamber.

Y.A. acknowledges the Marie Curie IOF support under the 7th framework program of the Commission of the European Community, Contract No. 221143. Helpful discussions of Y.A. with Dr. Zugang Mao of Northwestern University (Evanston, IL, USA) and with Dr. René Windiks of Materials Design Inc. are greatly appreciated.

[1]G. D. Wilk, R. M. Wallace, and J. M. Anthony, J. Appl. Phys. **89**, 5243 (2001).
[2]J. Robertson, Rep. Prog. Phys. **69**, 327 (2006).
[3]Y. Taur, International Workshop on Metal Gate/Work function Science and Engineering, University of California, San Diego, CA (2003).
[4]H. Zhong, S. N. Hong, Y. S. Suh, H. Lazar, G. Heuss, and V. Misra, Tech. Dig. – Int. Electron Devices Meet. **2001**, 467.
[5]I. Polishcuk, P. Ranade, T. J. King, and C. Hu, IEEE Electron Device Lett. **23**, 200 (2002).
[6]B. Y. Tsui and C. F. Huang, IEEE Electron Device Lett. **24**, 153 (2003).
[7]B. Chen, Y. Suh, J. Lee, J. Gurganus, V. Misra, and C. Cabral, Appl. Phys. Lett. **86**, 053502 (2005).
[8]T. Matsukawa, Y. X. Liu, M. Masahara, K. Ishii, K. Endo, H. Yamauchi, E. Sugimata, H. Takashima, T. Higashino, E. Suzuki, and S. Kanemaru, Microelectron. Eng. **80**, 284 (2005).
[9]T. L. Li, C. H. Hu, W. L. Ho, H. C. H. Wang, and C. Y. Chang, IEEE Trans. Electron Device **52**, 1172 (2005).
[10]C. H. Lu, G. M. T. Wong, M. D. Deal, W. Tsai, P. Majhi, C. O. Chui, M. R. Visokay, J. J. Chambers, L. Colombo, B. M. Clemens, and Y. Nishi, IEEE Electron Device Lett. **26**, 445 (2005).
[11]B. Chen, N. Biswas, and V. Misra, J. Electochem. Soc. **153**, G417 (2006).
[12]R. M. Todi, M. S. Erickson, K. B. Sundaram, K. Barmak, and K. R. Coffey, IEEE Trans. Electron Device **54**, 807 (2007).
[13]M. Sawkar-Mathur and J. P. Chang, J. Appl. Phys. **104**, 084101 (2008).
[14]M. S. Lee, C. H. An, K. Park, and H. Kim, Electrochem. Solid-State Lett. **12**, H120 (2009).
[15]C. H. Lu, G. M. T. Wong, R. Birringer, R. Dauskardt, M. D. Deal, B. M. Clemens, and Y. Nishi, J. Appl. Phys. **107**, 063710 (2010).
[16]S. Guha, V. K. Paruchuri, M. Copel, V. Narayanan, Y. Y. Wang, P. E. Batson, N. A. Bojarczuk, B. Linder, and B. Doris, Appl. Phys. Lett. **90**, 092902 (2007).
[17]H. N. Alshareef, M. Quevedo-Lopez, H. C. Wen, R. Harris, P. Kirsch, P. Majhi, B. H. Lee, R. Jammy, D. J. Lichtenwalner, J. S. Jur, and A. I. Kingon, Appl. Phys. Lett. **89**, 232103 (2006).
[18]L. Pantisano, T. Schram, B. O'Sullivan, T. Conard, S. De Gendt, G. Groeseneken, P. Zimmerman, A. Akheyar, M. M. Heyns, S. Shamuilla, V. V. Afanas'ev, and A. Stesmans, Appl. Phys. Lett. **89**, 113505 (2006).
[19]H. J. Li and M. I. Gardner, IEEE Electron Device Lett. **26**, 441 (2005).
[20]L. Kornblum, B. Meyler, C. Cytermann, S. Yofis, J. Salzman, and M. Eizenberg, Appl. Phys. Lett. **100**, 062907 (2012).
[21]H. B. Michaelson, J. Appl. Phys. **48**, 4729 (1977).
[22]M. V. Rossum, M. A. Nicolet, and W. L. Johnson, Phys. Rev. B **29**, 5498 (1984).
[23]H. Dadgour, K. Endo, V. K. De, and K. Banerjee, IEEE Trans. Electron Device **57**, 2504 (2010).
[24]M. E. Grubbs, X. Zhang, M. Deal, Y. Nishi, and B. Clemens, Appl. Phys. Lett. **97**, 223505 (2010).
[25]L. Kornblum, J. A. Rothschild, Y. Kauffmann, R. Brener, and M. Eizenberg, Phys. Rev. B **84**, 155317 (2011).
[26]J. Bardeen, Phys. Rev. **71**, 717 (1947).
[27]Y. C. Yeo, T. J. King, and C. Hu, J. Appl. Phys. **92**, 7266 (2002).
[28]J. Robertson, J. Vac. Sci. Technol. B **27**, 277 (2009).
[29]R. T. Tung, Phys. Rev. Lett. **84**, 6078 (2000).
[30]Y. T. Cheng, M. A. Nicolet, and W. L. Johnson, Mater. Res. Soc. Symp. **54**, 175 (1985).
[31]Y. T. Cheng, W. L. Johnson, and M. A. Nicolet, Appl. Phys. Lett. **47**, 800 (1985).
[32]K. H. J. Buschow, B. H. Verbeek, and A. G. Dirks, J. Phys. D **14**, 1087 (1981).
[33]H. Schroder, K. Samwer, and U. Koster, Phys. Rev. Lett. **54**, 197 (1985).
[34]Z. Radi, P. B. Barna, and J. Labar, J. Appl. Phys. **79**, 4096 (1996).
[35]K. Zeng, R. Stierman, T. C. Chiu, D. Edwards, K. Ano, and K. N. Tu, J. Appl. Phys. **97**, 024508 (2005).
[36]H. J. Fan, M. Knez, R. Scholz, D. Hesse, K. Nielsch, M. Zacharias, and U. Gosele, Nano Lett. **7**, 993 (2007)
[37]J. C. Barbour, A. E. M. J. Fischer, and J. F. van der Veen, J. Appl. Phys. **62**, 2582 (1987).
[38]H. Kim, P. C. McIntyre, C. O. Chui, K. C. Saraswat, and S. Stemmer, J. Appl. Phys. **96**, 3467 (2004).
[39]K. I. Seo, D. I. Lee, P. Pianetta, H. Kim, K. C. Saraswat, and P. C. McIntyre, Appl. Phys. Lett. **89**, 142912 (2006).
[40]C. Choi and J. C. Lee, J. Appl. Phys. **108**, 064107 (2010).
[41]*Instabilities in Silicon Devices*, edited by G. Barbottin and A. Vapaille (North-Holland, Amsterdam, The Netherlands, 1986).

[42]R. Jha, J. Gurganos, Y. H. Kim, R. Choi, J. Lee, and V. Misra, IEEE Electron Device Lett. **25**, 420 (2004).
[43]J. A. Rothschild, A. Shlomo, M. Eizenberg, B. Meyler, and J. Salzman, TowerJazz Tech. J. **1**, 85 (2011).
[44]Y. Kamimuta, K. Iwamoto, Y. Nunoshige, A. Hirano, W. Mizubayashi, Y. Wanatabe, S. Migita, A. Ogawa, H. Ota, T. Nabatame, and A. Toriumi, Tech. Dig. - Int. Electron Devices Meet. **2007**, 341.
[45]P. D. Kirsch, P. Sivasubramani, J. Huang, C. D. Young, M. A. Quevedo-Lopez, H. C. Wen, H. Alshareef, K. Choi, C. S. Park, B. H. Lee, and H. H. Tseng, Appl. Phys. Lett. **92**, 092901 (2008).
[46]M. Charbonnier, C. Leroux, V. Consier, P. Besson, F. Martin, G. Ghibaudo, and G. Reimbold, Microelectron. Eng. **86**, 1740 (2009).
[47]D. G. Delley, M. J. Swartzfager, and V. S. Sundaram, J. Vac. Sci. Technol. **16**, 664 (1979).
[48]S. C. Fain and J. M. McDavid, Phys. Rev. B **9**, 5099 (1974).
[49]M. Ropo, K. Kokko, L. Vitos, J. Kollar, and B. Johansson, Surf. Sci. **600**, 904 (2006).
[50]R. Bouwman, G. J. M. Lippits, and W. M. H. Sachtler, J. Catal. **25**, 350 (1972).
[51]W. M. H. Sachtler and G. J. H. Dorgelo, J. Catal. **4**, 654 (1965).
[52]Y. Takasu, H. Konno, and T. Yamashina, Surf. Sci. **45**, 321 (1974).
[53]K. Y. Yu, C. R. Helms, W. E. Spicer, and P. W. Chye, Phys. Rev. B **15**, 1629 (1977).
[54]R. Ishii, K. Matsumura, A. Sakai, and T. Sakata, Appl. Surf. Sci. **169–170**, 658 (2001).
[55]Y. S. Ng, T. T. Tsong, and S. B. McLane, Phys. Rev. Lett. **42**, 588 (1979).
[56]H. Y. Wang, R. Najafabadi, D. J. Srolovitz, and R. LeSar, Interface Sci. **1**, 7 (1993).
[57]R. Bouwman and W. M. H. Sachtler, J. Catal. **19**, 127 (1970).
[58]J. A. Rothschild and M. Eizenberg, Phys. Rev. B **81**, 224201 (2010).
[59]M. Yoshitake and K. Yoshihara, Appl. Surf. Sci. **146**, 97 (1999).
[60]M. Yoshitake, Y. Aparna, and K. Yoshihara, Appl. Surf. Sci. **169–170**, 666 (2001).
[61]T. C. Leung, C. L. Kao, W. S. Su, Y. J. Feng, and C. T. Chan, Phys. Rev. B **68**, 195408 (2003).
[62]S. Park, L. Colombo, Y. Nishi, and K. Cho, Appl. Phys. Lett. **86**, 073118 (2005).
[63]H. R. Gong and K. Cho, Appl. Phys. Lett. **91**, 092106 (2007).
[64]H. R. Gong, Y. Nishi, and K. Cho, Appl. Phys. Lett. **91**, 242105 (2007).
[65]G. Xu, Q. Wu, Z. Chen, Z. Huang, R. Wu, and Y. P. Feng, Phys. Rev. B **78**, 115420 (2008).
[66]B. Magyari-Kope, S. Park, L. Colombo, Y. Nishi, and K. Cho, J. Appl. Phys. **105**, 013711 (2009).
[67]G. Xu, Q. Wu, Z. Chen, Z. Huang, and Y. P. Feng, J. Appl. Phys. **106**, 043708 (2009).
[68]F. R. de Boer, R. Boom, W. C. M. Mattens, A. R. Miedema, and A. K. Niessen, *Cohesion in Metals* (North-Holland, Amsterdam, 1988).
[69]*CRC Handbook of Chemistry and Physics*, 87th ed., edited by D. R. Lide (CRC, Boca Raton, FL, 2007).
[70]Y. Jiang and J. R. Smith, J. Mater. Sci. **44**, 1734 (2009).
[71]R. G. Parr and W. Yang, *Density-Functional Theory of Atoms and Molecules*, (Oxford University Press, New York, 1989).
[72]R. M. Martin, *Electronic Structure—Basic Theory and Practical Methods*, (Cambridge University Press, Cambridge, UK, 2004).
[73]Y. Mishin, M. Asta, and J. Li, Acta Mater. **58**, 1117 (2010).
[74]G. Kresse and J. Furthmuller, Comput. Mater. Sci. **6**, 15 (1996).
[75]G. Kresse and J. Furthmuller, Phys. Rev. B **54**, 11169 (1996).
[76]G. Kresse and J. Hafner, Phys. Rev. B **49**, 14251 (1994).
[77]G. Kresse and D. Joubert, Phys. Rev. B **59**, 1758 (1999).
[78]W. Kohn and L. J. Sham, Phys. Rev. **140**, A1133 (1965).
[79]R. P. Feynman, Phys. Rev. **56**, 340 (1939).
[80]H. T. Takeshita, T. Oishi, and N. Kuriyama, J. Alloys Compd. **333**, 266 (2002).
[81]R. Y. Qi and J. D. Corbett, Inorg. Chem. **33**, 5727 (1994).
[82]X. D. Liu, X. B. Liu, and Z. Altounian, Acta Mater. **53**, 1439 (2005).
[83]Y. Amouyal, Z. Mao, and D. N. Seidman, Acta Mater. **58**, 5898 (2010).
[84]Y. Amouyal, Z. Mao, and D. N. Seidman, Appl. Phys. Lett. **93**, 201905 (2008).
[85]H. Zhu, M. Aindow, and R. Ramprasad, Phys. Rev. B **80**, 201406(R) (2009).
[86]H. L. Skriver and N. M. Rosengaard, Phys. Rev. B **46**, 7157 (1992).
[87]C. D. Yang, W. Li, and W. Zhi, Solid State Commun. **151**, 1270 (2011).